2018

Intermediate Vapor Bypass: A Novel Design for Mobile Heat Pump at Low Ambient Temperature

Lili Feng
University of Illinois at Urbana-Champaign, United States of America, lfeng8@illinois.edu

Predrag S. Hrnjak
pega@illinois.edu

Intermediate Vapor Bypass: A Novel Design for Mobile Heat Pump at Low Ambient Temperature

Lili Feng[1]*, Pega Hrnjak[1,2]

[1]University of Illinois at Urbana-Champaign, Department of Mechanical Science and Engineering, Champaign, Illinois, United States
lfeng8@illinois.edu

[2]Creative Thermal Solutions,
Urbana, Illinois, United States
pega@illinois.edu

* Corresponding Author

ABSTRACT

With market share of electric vehicles continue to grow, there is an increasing demand of mobile heat pump for cabin climate control, as it has much higher energy efficiency than electric resistive heating and hence much less impact on electric drive range. However, current mobile heat pump systems using low pressure refrigerants like R134a and R1234yf suffer from significant heating capacity loss at low ambient temperature. As a result, a large electric heater needs to be installed to supplement the capacity shortage at low ambient temperature, and electric drive range can be greatly reduced due to large power consumption for cabin heating. In this paper, the drop of heating capacity at low ambient temperature was experimentally and numerically studied. Pressure drop and refrigerant maldistribution in the outdoor heat exchanger in HP mode were found to be the most important factors. A novel design of the outdoor heat exchanger using intermediate vapor bypass in HP mode and the corresponding system architecture were proposed. The proposed outdoor heat exchanger turns into a condenser with integrated receiver and subcooler in A/C mode. A proof-of-concept heat exchanger prototype was made by modifying the baseline heat exchanger and tested in the lab. The result has shown 35% improvement of heating capacity at -20℃ ambient condition. Optimization of the outdoor heat exchanger design was investigated with a system model.

1. INTRODUCTION

According to the data reported from insideevs.com, as shown in Figure 1(a), sales of electric vehicles (EV) has been growing rapidly both in the US and in the world markets. In 2017, the total sales of passenger EV's has breached one million units. Figure 1(b) shows the EPA rated drive range of the best-selling EV models in the US in 2017, based on the data provided by fueleconomy.gov. The market has developed into two branches: a longer range group having drive range over 200 miles, and a shorter range group with about 100 miles of range. There is a clear trend that longer range models usually get better sales. While limited drive range is posing great challenge to the EV market, cabin climate control, especially heating during winter, is intensifying the range anxiety. Numerous studies have shown 40~60% of drive range reduction in cold weather, when a positive temperature coefficient (PTC) electric heater is used to convert battery electricity into heat. Compared to PTC heaters, heat pump is a much more efficient way of providing heat. Currently, several EV models have started using heat pump for cabin heating, including Renault Zoe, Nissan Leaf, BMW i3, Kia Soul, Volkswagen E-Golf, Hyundai Ioniq, and Toyota Prius Prime Plug-in Hybrid. Some of them have reported 20~30% of drive range increase in cold ambient.

Although many different mobile heat pump configurations using different refrigerants have been developed in the literature, most of them cannot provide enough heat at very low ambient temperature. For a list of heat pump systems, Table 1 shows the lowest tested ambient temperature and the maximum heating capacity obtained at that ambient condition. As the table shows, R134a was tested only down to -15℃. At -20℃, the CO_2 system developed by Denso was able to supply 5.0 kW of heating capacity. Nevertheless, no details of this system were given except that it was designed for a fuel cell hybrid vehicle (FCHV). The systems from Behr and Visteon using R1234yf were only able to

provide less than 3 kW of heat when ambient temperature reached -20℃. At the same ambient condition, the system from CTS using a wide glide blend (WGB) provided 3.6 kW of heating capacity, benefiting from higher evaporating pressure. However, noticeable performance degradation in A/C mode has been reported.

In this paper, heating performance of a direct expansion (DX) heat pump system using R1234yf was investigated at ambient temperatures from 20℃ to -20℃. The baseline system provided 2.48 kW of heating capacity at -20℃. Challenges of heat pumping at low ambient temperature were looked into experimentally and numerically with the help of a system model developed by Feng and Hrnjak (2016). Without changing to a higher pressure refrigerant, intermediate vapor bypass (IVB), a new heat exchanger and system design concept was presented. By a proof-of-concept IVB modification of the outdoor heat exchanger, heating capacity at the same operating condition was improved by 35% to 3.36 kW. Further improvement of outdoor heat exchanger design was examined using the system model, and experimental validation was underway.

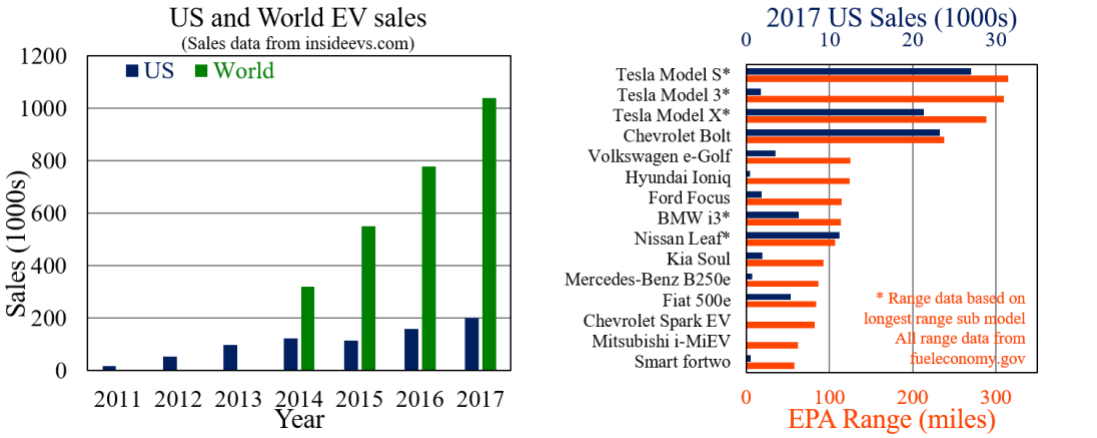

(a). EV sales in the US and in the world (b). Greater range models tend to get better sales

Figure 1. EV market rapidly growing and favors longer range models

Table 1. Heat pump systems in the literature

System	Type	Ref	$T_{amb,min}$	Load	Q_{max}	HPF
-	-	-	℃	kW	kW	-
Suzuki and Ishii 1996, Denso	DX	R134a	-10	5.5	2.3	2.3
Giannavola et al. 2000, ACRC	DX	CO_2	-10	-	3.8	3.5
Werner et al. 2003, Denso*	DX	CO_2	-20	-	5.0	-
Antonijevic and Keckt 2004, Visteon	DX	R134a	-11	-	1.9	-
Wawzyniak 2011, Behr	DX	R134a	-10	3.6	3.7	2.2
Wawzyniak 2011, Behr	DX	R1234yf	-20	4.7	2.9	2
Wawzyniak 2011, Behr	Hybrid	R1234yf	-20	4.7	2.8	2
Kowsky et al. 2012, Delphi	SL	R134a	-10	6.5	4	2.3
Benouali et al. 2012, Visteon	DX	R1234yf	-18	-	2.7	2.35
Benouali et al. 2012, Visteon	Hybrid	R1234yf	-18	-	2.7	2.03
Musser et al. 2012, CTS	DX	R134a	-15	-	3.2	1.85
Musser et al. 2012, CTS	DX	WGB	-20	-	3.6	1.75

* no details of the tests were found. System designed for fuel cell hybrid vehicle (FCHV)

2. BASELINE SYSTEM PERFORMANCE AND ANALYSIS

The baseline system is a three heat exchanger DX system using all microchannel heat exchangers. Figure 2 shows the system configuration and testing facility. In a previous paper, Feng and Hrnjak (2016) has given a detailed description of the system architecture, as well as basic heating performance characteristics of the system at various operating conditions. Also, a significant refrigerant charge imbalance when switching between cooling mode and heating mode has been noticed. In this paper, the attention was focused on heating performance at different ambient temperatures, especially on the challenges at extremely low ambient temperature.

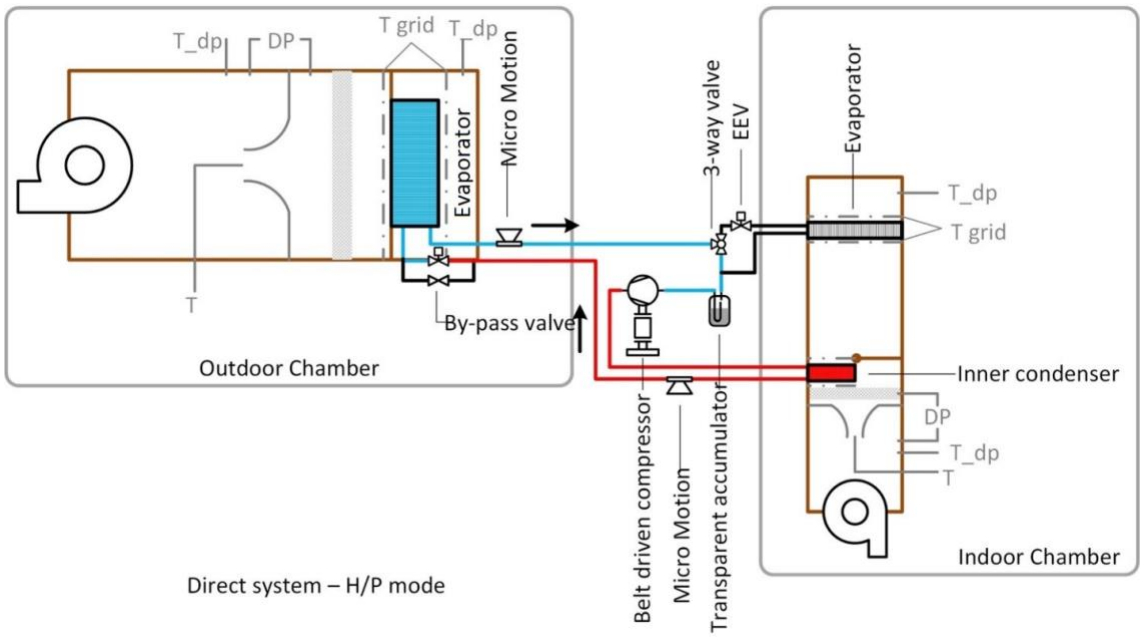

Figure 2. Baseline system in test facility

For a series of steady state dry conditions using R1234yf, the ambient temperatures was varied from 20℃ to -20℃, the indoor air inlet temperature was set to be the same as ambient to imitate cold-soak start-up or 100% outside air ventilation condition. The indoor air discharge temperature target was arbitrarily set at 50℃. Indoor air flow rate was fixed at 6 kg/min, and outdoor heat exchanger face velocity was maintained at 4 m/s. With a 135 cm^3 displacement, the maximum compressor speed was set to 2000 rpm to match the maximum volumetric capacity of a reasonably sized electric compressor. In addition, subatmospheric suction was not allowed to prevent non-condensable and moisture from leaking into the system. For each operating condition, the compressor speed was gradually increased until indoor discharge temperature reached the target, or suction pressure reached atmosphere, or compressor speed reached maximum, whichever happened first. An electronic expansion valve (EEV) was used to manually maintain inner condenser outlet subcooling at 18℃ for close to optimum heating performance factor (HPF) based on results from Feng and Hrnjak (2016). The system was charged until there was about 150 g of refrigerant liquid in the accumulator, imitating a mildly overcharged situation in HP mode. As a result, the suction quality was about 95%.

Figure 3(a)~(c) shows the system heating performance and operating parameters at different ambient temperatures. At higher ambient temperatures from 20℃ to 5℃, the system was able to reach the 50℃ discharge air target with reduced compressor speed. For ambient temperature between 0℃ and -15℃, as the temperature lift required to reach the discharge target was increasing, the needed heating capacity was linearly increasing. However, with compressor speed reached maximum, the realized heating capacity kept decreasing with dropping ambient temperature, deviating from the needed capacity. This capacity drop was mainly caused by the drop of suction density and the resulting lower refrigerant mass flow rate. The relationships were given in Eq. (1) and Eq. (2). Calculating at the same evaporating temperatures as measured, the normalized saturated vapor density of four different refrigerants were shown in Figure 3(d), including a high pressure fluid CO_2, a medium pressure fluid R32, and two low pressure fluids R134a and R1234yf. As a matter of fact, the relative drop of suction density at lower ambient temperature for higher pressure refrigerants was only slightly less than that for low pressure refrigerants. In other words, when compressor size is the limitation, changing to a higher pressure refrigerant won't significantly reduce the heating capacity loss at low ambient temperature. When ambient temperature reached -20℃, the system heating capacity dropped largely to 2.48 kW. The additional capacity drop was a result of reduced compressor speed. As suction pressure lowered at lower ambient temperature, the compressor speed had to be restricted at 62% to prevent vacuum suction at -20℃ ambient, when heating capacity was most needed. This limitation only exists for low pressure refrigerants. In fact, when the same experiment at -20℃ was ran with R134a, a slightly lower pressure fluid compared to R1234yf, the compressor speed was restricted even further to 45% to keep suction pressure slightly above atmosphere, and the system heating capacity dropped to 2.0 kW.

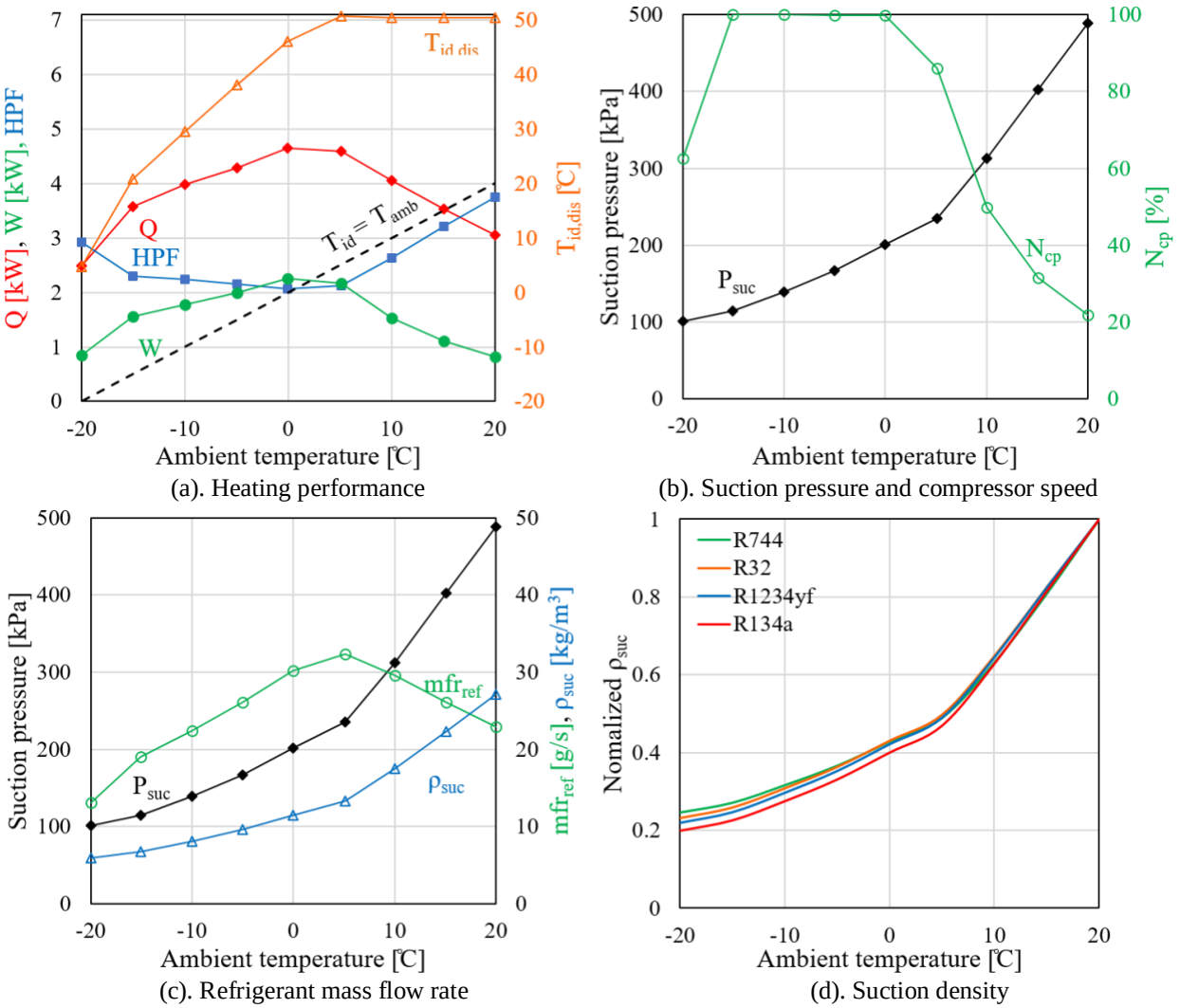

(a). Heating performance

(b). Suction pressure and compressor speed

(c). Refrigerant mass flow rate

(d). Suction density

Figure 3. Baseline performance characteristics

$$Q = \dot{m}_{ref} \cdot \Delta h_{ic} \tag{1}$$

$$\dot{m}_{ref} = \frac{V_{disp} N_{cp} \eta_{vol} \rho_{suc}}{60} \tag{2}$$

The third limitation on heating capacity was refrigerant maldistribution in the outdoor heat exchanger, especially in the second pass. Figure 4(a) shows the frosted outdoor heat exchanger while moisture was arbitrarily added into the environmental chamber. The non-uniform frost pattern indicated serious refrigerant two phase maldistribution among the second larger pass. The effect was evaluated using the system model and a heat exchanger maldistribution model. By assuming the thermal resistance to be air-side dominant, the frosted length profile was used directly as the input for liquid refrigerant mass flow rate distribution profile, and vapor mass flow rate through each microchannel in the second pass was iteratively adjusted until pressure at the heat exchanger outlet equalized. The resulting refrigerant temperature inside the outdoor heat exchanger in Figure 4(b) clearly shows the unfrosted surface has refrigerant temperature almost equal to ambient air temperature of -20℃. These surfaces had neglibigle contribution to heat transfer from air to refrigerant. Simply by assuming uniform distribution in the second pass in the model, the compressor speed was increased to 80% before having vacuum suction, and heating capacity was increased to 3.0 kW.

Figure 4(b) also shows that refrigerant temperature close to the entrance of the first smaller pass was only slightly lower than air temperature. In fact, there was a huge temperature glide of refrigerant due to pressure drop in the outdoor

heat exchanger. Figure 4(c) shows the refrigerant saturation temperature and average temperature across the 29 tubes in the second pass along the flow length. The temperature glide from pressure drop in the outdoor heat exchanger was 8℃, while the maximum air-to-refrigerant temperature difference was only 9.5℃. As a result, there was a much smaller effective temperature difference that's driving heat transfer from ambient air to refrigerant. This large temperature glide was a result of high sensitivity of saturation temperature to pressure at low evaporating temperature. The sensitivity can be estimated using the Clausius-Claypeyron relation, as shown in Eq. (3). For low pressure fluid at extremely low evaporating temperature, saturated vapor density become much smaller, hence resulting in much greater temperature glide for the same amount of pressure drop. Table 2 shows that higher pressure fluid R32 and CO_2 has much smaller dT/dP values, hence much less likely to suffer from huge temperature glide from pressure drop.

$$\left(\frac{dT}{dP}\right)_{sat} = \frac{v_{fg}}{s_{fg}} \approx \frac{v_g}{s_{fg}} = \frac{T}{\rho_g \cdot h_{fg}} \tag{3}$$

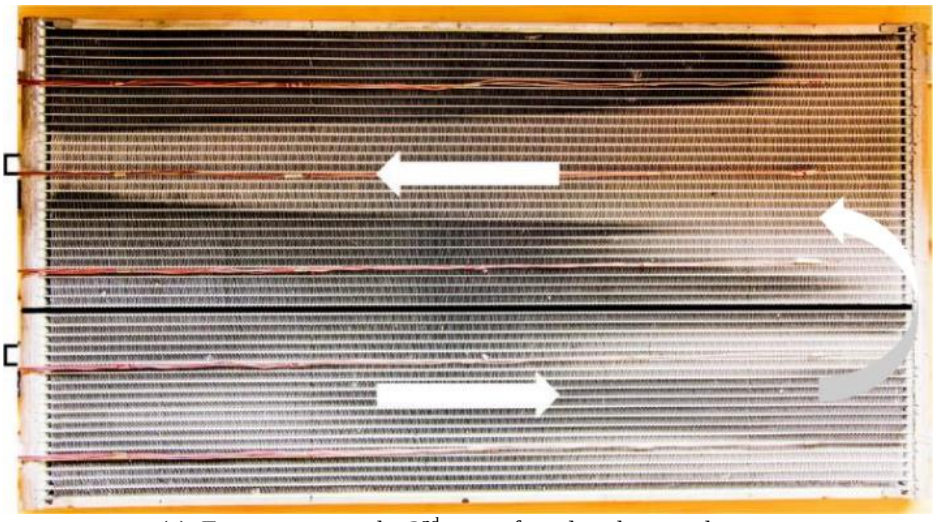

(a). Frost pattern at the 2nd pass of outdoor heat exchanger

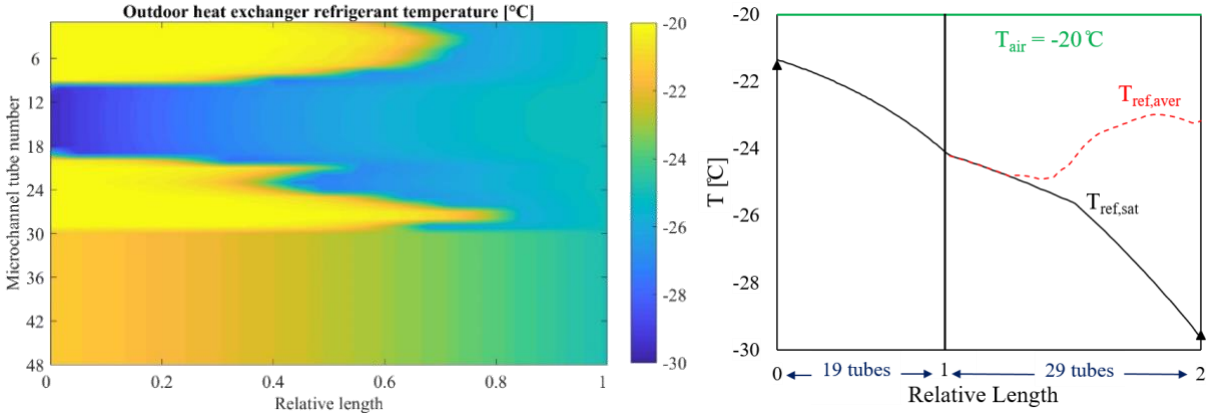

(b). Refrigerant temperature distribution (c). Temperature glide in the outdoor heat exchanger

Figure 4. Refrigerant maldistribution and temperature glide in the outdoor heat exchanger

Table 2. Temperature sensitivity to pressure of different refrigerants

@ -29.5℃	R134a	R1234yf	R32	CO2
P [kPa]	86.4	101.3	279.1	1451
ρ_g [kg/m3]	4.5	6.0	7.8	37.7
h_{fg}[kJ/kg-K]	219.2	180.3	356.2	302.5
dT/dP [K/kPa]	0.2448	0.2251	0.0872	0.0206

3. INTERMEDIATE VAPOR BYPASS: CONCEPT AND RESULTS

Without changing to a higher pressure fluid, refrigerant maldistribution and temperature glide from pressure drop in the outdoor heat exchanger need to be reduced in order to improve heating capacity at extremely low ambient temperature. Flash gas bypass (FGB) was intensively studied since it was first introduced to a smaller scale CO_2 A/C system by Beaver et al. (1999). Later on, Elbel and Hrnjak (2003) and Tuo and Hrnjak (2012) have reported significant COP and cooling capacity improvement for CO_2 and R134a mobile air conditioning (MAC) systems, and they attributed the benefits of FGB to more uniform refrigerant distribution and less pressure drop in the evaporator.

Intermediate vapor bypass is an adaption of FGB for reversible AC/HP system. Figure 5 shows a two pass reversible outdoor heat exchanger design in HP and A/C modes. In HP mode, two phase refrigerant after the expansion valve enters the outdoor heat exchanger from the smaller pass. After some evaporation, the two phase fluid enters the intermediate separator and vapor is bypassed through the bypass valve, while only liquid is sent to the second larger pass for further evaporation. When the system is switched to A/C mode, refrigerant enters the outdoor heat exchanger from the larger pass. With bypass valve closed, the separator becomes a receiver, and the smaller pass becomes a subcooler. Essentially, the outdoor heat exchanger becomes an integrated receiver subcooler condenser that's widely acknowledged as a good condenser design in the automotive industry. The four check valves between the two passes and separator/receiver work like an electric bridge circuit, and ensures that refrigerant always enters the separator receiver from the side port, while exits from the bottom as liquid. Figure 6 shows the system architecture design with the proposed reversible outdoor heat exchanger. Compared to the baseline system, the suction accumulator was replaced with the separator receiver, only one extra bypass valve is needed, while all other components remain the same or only need slight modifications.

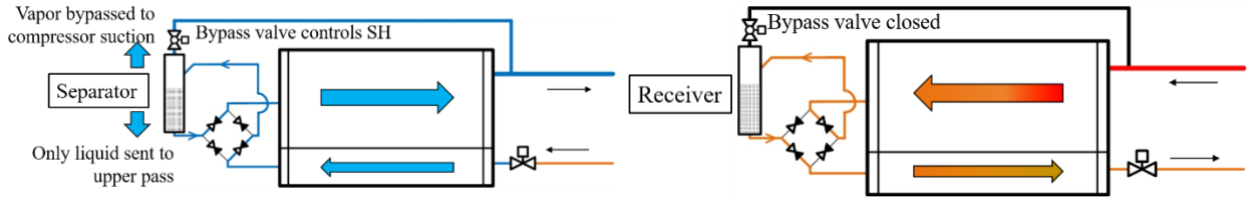

(a). HP mode intermediate vapor bypass evaporator (b). A/C mode integrated receiver condenser

Figure 5. New reversible outdoor heat exchanger design

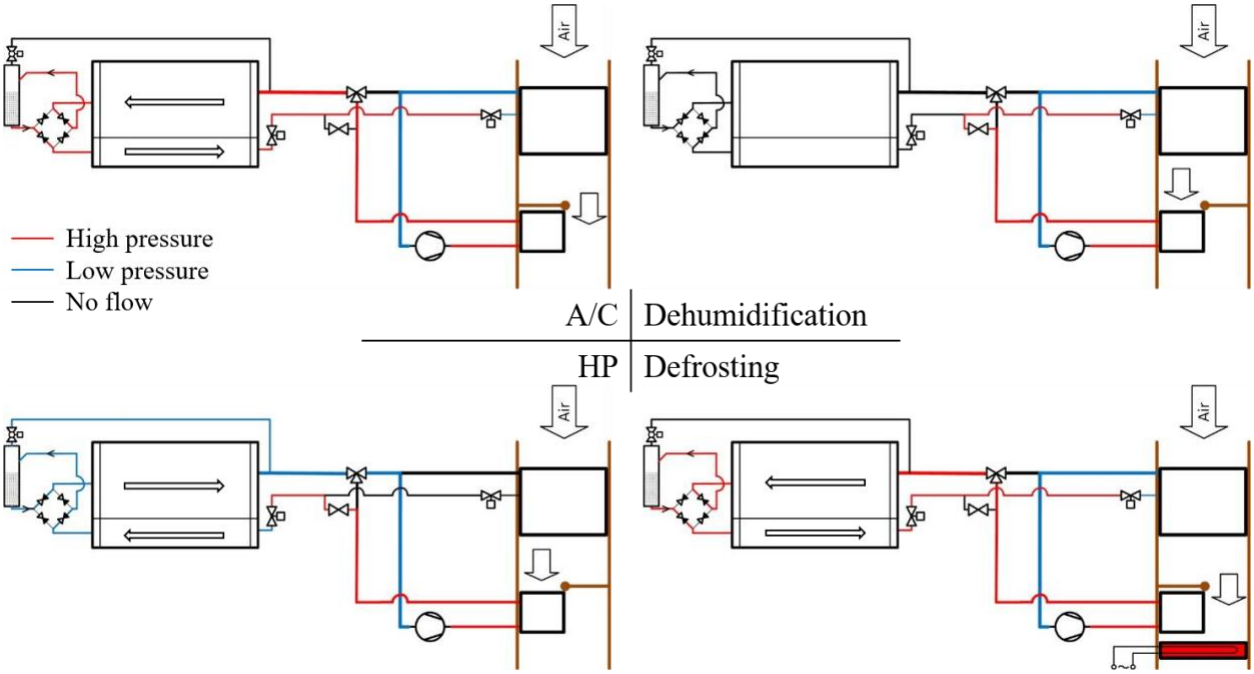

Figure 6. System architecture and operating modes with new outdoor heat exchanger design

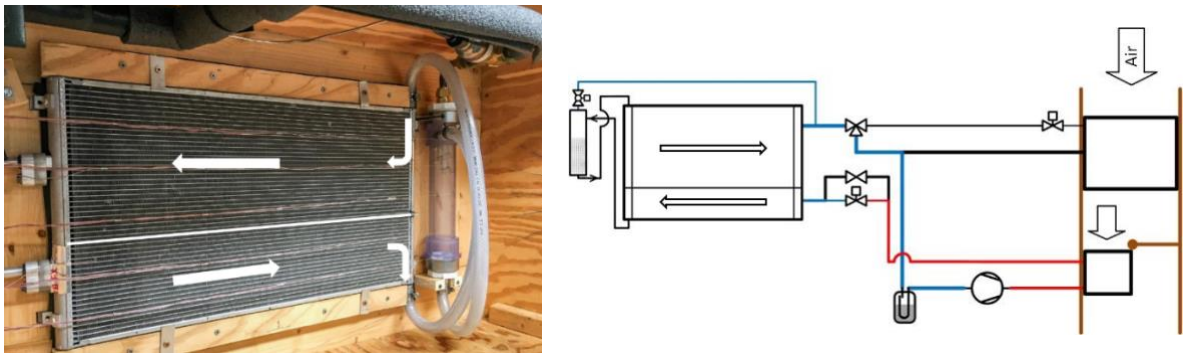

(a). Intermediate vapor bypass modified outdoor heat exchanger (b). Proof-of-concept system modification

Figure 7. Proof-of-concept heat exchanger and system modification

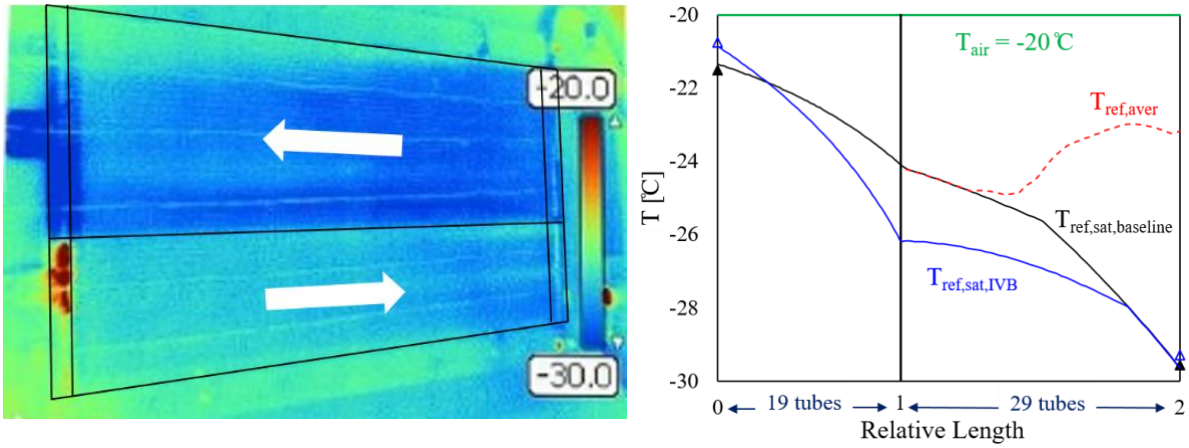

(a). Improved refrigerant distribution (b). Improved refrigerant temperature profile

Figure 8. Improvements from intermediate vapor bypass

Table 3. Performance improvement using intermediate vapor bypass

$T_{id} = T_{amb}$ = -20 [℃], mfr_{ida} = 6[kg/min], Vel_{ohex} = 4[m/s], SC = 18 [℃] Data / Model

Configuration	Baseline Mal 19 | 29	Baseline Uni 19 | 29	IVB w/ accu 19 | 29	IVB w/ accu 4+4 | 38	IVB w/o accu 4+4 | 38
P_{cpri} [kPa]	101.0 / 101.3	101.3	102.2 / 103.1	106.3	107.2
P_{cpro} [kPa]	596.0 / 503.6	604.3	686.5 / 729.6	750.7	783.4
N_{cp} [%]	**63** / 62	80	**100** / 100	100	100
$T_{id,dis}$ [℃]	**5.2** / 5.2	10.1	**13.9** / 15.4	16.1	18.0
$Q_{heating}$ [kW]	**2.52** / 2.53	3.02	**3.36** / 3.56	3.63	3.82
W_{shaft} [kW]	0.85 / 0.64	0.87	1.39 / 1.17	1.21	1.30
Q_{oh} [kW]	1.61 / 1.89	2.15	2.20 / 2.40	2.46	2.58
HPF [-]	2.96 / 3.97	3.47	2.42 / 3.03	3.01	2.93
$\dot{m}_{ref}$ [g/s]	13.1 / 13.6	16.4	17.6 / 19.6	20.2	20.0
DP_{ohr} [kPa]	34.0 / 35.9	44.1	36.0 / 43.5	15.6	16.5

In order to verify the potential benefit with intermediate vapor bypass, the outdoor heat exchanger was modified by adding a separator between the two flow passes, while the rest of the baseline system was kept the same, as shown in Figure 7. With this setup, experiments were ran at the exact same conditions as the baseline for -20℃ ambient.

Infrared image of the outdoor heat exchanger in Figure 8(a) shows much more uniform refrigerant distribution in the second pass when vapor was bypassed and only liquid was supplied for further evaporation. By sending less refrigerant mass flow rate and lower inlet quality to the second pass, refrigerant pressure drop and the resulting temperature glide in the second pass was reduced, and greater air-to-refrigerant temperature difference was obtained, as shown in Figure 8(b). Both factors contributed to a better performing outdoor heat exchanger. The measured operating parameters of the baseline and the intermediate vapor bypass system were listed in Table 3. The data showed that by bypassing vapor from the intermediate separator, heating capacity of the system increased by 35% to 3.36 kW. Moreover, the compressor speed was able to reach 100% while suction pressure was still slightly higher than atmospheric pressure.

4. FUTHUR IMPROVEMENT OPPORTUNITIES

The current proof-of-concept modification kept the original pass circuitry of 19 tubes in the smaller pass and 29 tubes in the larger pass. When the system is switched to A/C mode, the outdoor heat exchanger becomes a condenser, and the smaller pass with 19 tubes works as a subcooler. However, sizing of the subcooler can be critical for A/C performance. By changing the number of tubes in the smaller pass, and running the system model in A/C mode under M35 condition according to SAE Standard J2765, the system cooling capacity and coefficient of performance (COP) were obtained and plotted in Figure 9(a). Apparently, for greater cooling capacity and COP, size of the smaller pass should be reduced to about 10 tubes. Similarly, for HP mode at -20℃ ambient, in order to maximize heating capacity, size of the smaller pass should be reduced as much as possible, because intermediate vapor bypass primarily improves performance of the second larger pass. However, when the smaller pass was reduced to 10 tubes, the temperature glide from pressure drop in the smaller pass became so large that the refrigerant inlet temperature became greater than air inlet temperature, contributing negatively on heat collecting capacity, as shown in Figure 10(a). A simple fix is to use larger hydraulic diameter microchannel tubes in the smaller pass. By doubling the hydraulic diameter and reducing the number of ports accordingly, temperature glide in the first pass can be effectively reduced, and heating capacity can be further increased to 3.7 kW, although A/C cooling capacity and COP may slightly drop due to lower mass flux and lower heat transfer coefficient in the subcooled region. A prototype heat exchanger using two slabs of four larger hydraulic diameter tubes in parallel as the smaller pass and 38 original microchannel tubes as the larger pass is currently being built for experimental validation, as shown in Figure 10(b). The heat exchanger part for the smaller pass was carefully selected so that face area and total air side heat transfer area were maintained close to the baseline heat exchanger, while refrigerant cross-sectional area in the smaller pass was increased. Simulation results were shown in the last two columns in Table 3. By using this design, and eliminating the accumulator, heating capacity at -20℃ ambient was expected to reach 3.8 kW.

In the new prototype, a new reversible separator was made with integrated check valves. Since the check valves only work with small pressure difference within the two passes of the outdoor heat exchanger, they can be made cheaply with plastics and put inside the pressure bearing separator/receiver. A 3D printed insert with integrated flap valves was fabricated and integrated into the separator. For manufacturing, the reversible outdoor heat exchanger can be brazed in the same way as conventional integrated receiver subcooler condenser, while a separately manufactured plastic valve bridge insert can be assembled into the separator/receiver. Eventually, the reversible outdoor heat exchanger looks very similar to an integrated receiver subcooler condenser, as shown in Figure 11.

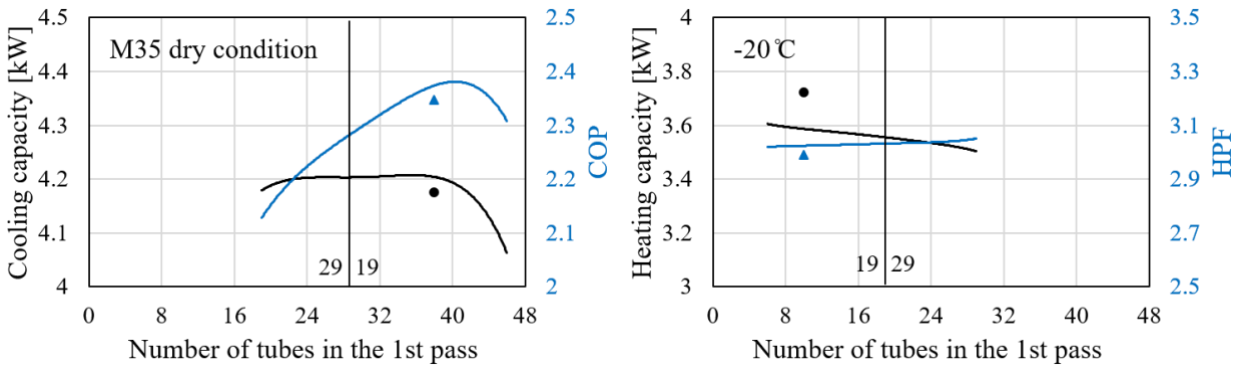

(a). A/C mode as a condenser (b). HP mode as an evaporator

Figure 9. Outdoor heat exchanger pass optimization (dots are for doubled hydraulic diameter of the smaller pass)

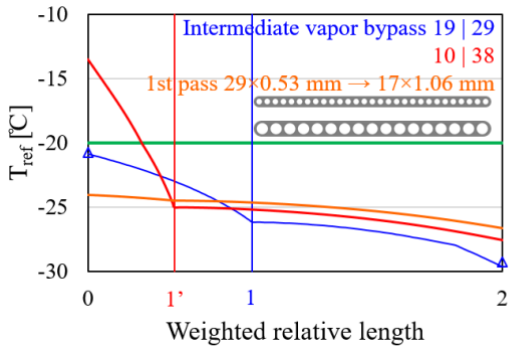

(a). Using larger diameter tube for the smaller pass (b). Prototyping with two different tube geometries

Figure 10. Outdoor heat exchanger pass design improvement

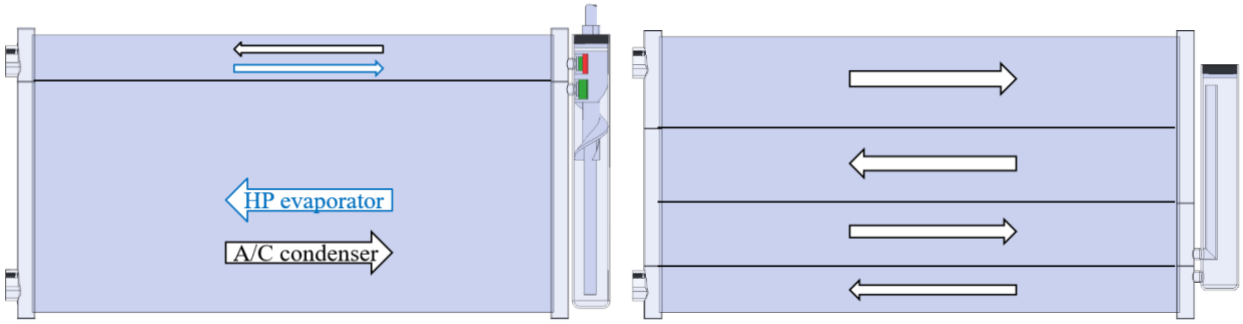

(a). Reversible outdoor heat exchanger design (b). Commonly seen integrated receiver subcooler condenser

Figure 11. Outdoor heat exchanger design

5. CONCLUSIONS

Current heat pump system for electric vehicles using low pressure refrigerant suffer from significant heating capacity loss at extremely low ambient temperature, primarily due to four factors:

- Lower suction density at lower evaporating temperature causes lower refrigerant mass flow rate
- As suction pressure approaches atmospheric pressure, compressor speed needs to be lowered
- Refrigerant maldistribution deteriorates the outdoor heat exchanger performance
- Pressure drop in the outdoor heat exchanger results in large temperature glide

By bypassing vapor with an intermediate separator between the two flow passes of the outdoor heat exchanger, significant improvement of refrigerant two phase distribution was achieved, as well as largely reduced refrigerant pressure drop and temperature glide in the larger pass. These two factors helped to bring the compressor speed to 100% without getting suction pressure below atmosphere. Eventually, the proof-of-concept intermediate vapor bypass modified system achieved 3.36 kW of heating capacity, a 35% increase compared to the 2.48 kW provided by the baseline system.

To fully incorporate intermediate vapor bypass in HP mode, the outdoor heat exchanger pass design need to be improved to ensure good performance in A/C mode, when the outdoor heat exchanger becomes an integrated receiver condenser. Preliminary simulation results has shown a favor towards a reduced small pass, while the hydraulic diameter in this smaller pass should be increased to reduce pressure drop in HP mode. A prototype is being built using two different hydraulic dimeter heat exchangers. While refrigerant side cross-sectional area in the smaller pass is increased, air side face area and heat transfer area are carefully matched. By using the system model for this more reasonably designed reversible outdoor heat exchanger with intermediate vapor bypass in HP mode, the system heating capacity is expected to reach about 3.8 kW. Experimental evaluation of the prototype will be carried out in the near future.

NOMENCLATURE

A/C	air conditioning
COP	coefficient of performance, $Q_{cooling}/W_{cp,shaft}$
DX	direct expansion
EEV	electronic expansion valve
EV	electric vehicle
HP	heat pump
HPF	heating performance factor, $Q_{heating}/W_{cp,shaft}$
MAC	mobile air condioning
PTC	positive temperature coefficient
SL	secondary loop

accu	accumulator
cp	compressor
ic	inner condenser
disp	displacement
suc	suction
a/r	air side/refrigerant side
i/o	inlet/outlet
f	liquid phase
g	gas phase
id/od	indoor/outdoor
η_{vol}	volumetric efficiency

REFERENCES

Antonijevic, D., and Heckt, R., (2004). Heat Pump Supplemental Heating System for Motor Vehicles. *Proc. Instn Mech. Engrs*.

Beaver, A.C., Yin, J.M., Bullard, C.W., Hrnjak, P.S., (1999). An experimental investigation of transcritical carbon dioxide systems for residential air-conditioning. *ACRC Report CR-18*.

Benouali, J., (2012). Heat Pump Architectures for Electrified Cars. *SAE Thermal Management Systems Symposium*.

Elbel, S. and Hrnjak, P., (2004). Flash gas bypass for improving the performance of transcritical R744 systems that use microchannel evaporators. *Int. J. Refrigeration 27 (2004) 724-735*.

Tuo, H. and Hrnjak, P., (2012). Flash gas bypass in mobile air conditioning system with R134a. *Int. J. Refrigeration 35 (2012) 1869-1877*.

Feng, L. and Hrnjak, P., (2016). Experimental Study of an Air Conditioning-Heat Pump System for Electric Vehicles. *SAE Int. J. Passeng. Cars - Mech. Syst. 9(1)*.

Feng, L. and Hrnjak, P., (2016). Experimental and Numerical Study of a Mobile Reversible Air Conditioning-Heat Pump System. *16th International Refrigeration and Air Conditioning Conference*. Paper 2569.

Giannavola, M.S., Murphy, R., Yin, J.M., Bullard, C.W., Hrnjak, P.S., (2000). Experimental Comparison of R134a and Transcritical CO2 Mobile Heat Pump and A/C Systems and the Feasibility of a Transcritical CO2 Heat Pump for a Sport Utility Vehicle. *4th IIR Gustav Lorentzen Conference*.

Musser, A. and Hrnjak, P. S., (2014). Mobile Heat Pump Exploration Using R445A and R744. *International Refrigeration and Air Conditioning Conference*. Paper 1514.

Kowsky, C., Wolf, E., Leitzel, L., Oddi, F., (2012). Unitary HPAC System. *SAE Int. J. Passeng. Cars -Mech. Syst*.

Wawzyniak, M., (2011). Benefits and Challenges of Heat Pump Systems. *SAE Alternate Refrigerant Systems Symposium*, presentation.

Werner, H., and Kakehashi, N., (2003). CO2 Heat Pump System with Electric Compressor. *VDA Alternative Refrigerant Winter Meeting*.

SAE International Surface Vehicle Standard, (2008). Procedure for Measuring System COP [Coefficient of Performance] of a Mobile Air Conditioning System on a Test Bench, *SAE Standard J2765*.

Suzuki, T. and K. Ishii, (1996). Air Conditioning System for Electric Vehicle. *SAE Technical Paper 960688*.

ACKNOWLEDGEMENT

This work was supported by the Air Conditioning and Refrigeration Center at the University of Illinois at Urbana-Champaign. All help from center members and sponsor companies are gratefully acknowledged!